Coherent quantum transport in narrow constrictions in the presence of a finite-range longitudinally polarized time-dependent field

C. S. Tang and C. S. Chu
Department of Electrophysics, National Chiao Tung University, Hsinchu 30010, Taiwan, Republic of China
(Received 23 October 1998; revised manuscript received 1 February 1999)

We have studied the quantum transport in a narrow constriction acted upon by a finite-range longitudinally polarized time-dependent electric field. The electric field induces coherent inelastic scatterings that involve both intrasubband and intersideband transitions. Subsequently, the dc conductance G is found to exhibit suppressed features. These features are recognized as the quasi-bound-state (QBS) features that are associated with electrons making transitions to the vicinity of a subband bottom, of which the density of states is singular. Having valleylike instead of diplike structures, these QBS features are different from the G characteristics for constrictions acted upon by a finite-range time-modulated potential. In addition, the subband bottoms in the time-dependent electric-field region are shifted upward by an energy proportional to the square of the electric field and inversely proportional to the square of the frequency. This effective potential barrier is originated from the square of the vector potential, and it leads to the interesting field-sensitive QBS features. An experimental setup is proposed for the observation of these features. [S0163-1829(99)01827-5]

Quantum transport in mesoscopic systems has received much attention in recent years. Among the most studied mesoscopic structures is the quantum point contact (QPC), due to its simple configuration. In such QPC systems, the lateral energy is quantized into subbands, giving rise to a quantized conductance G.[1–3] These QPC's can be created electrostatically by negatively biasing the split gates located on top of a GaAs-$Al_xGa_{1-x}As$ heterostructure.[1–3]

The QPC can be pictured as a narrow constriction connecting adiabatically at each end to a two-dimensional electron gas (2DEG),[4,5] as depicted in Fig. 1. The energy levels in the narrow constriction are quantized into one-dimensional subbands, which density of states (DOS) is singular at a subband bottom. In the presence of an attractive scatterer, such singular DOS gives rise to dip structures in G,[6–12] which is associated with the impurity-induced quasiband states[7] (QBS's) formed just beneath a subband bottom.

Recently, there has been growing interest in the time-dependent responses of QPC structures. The time-dependent fields that act upon the QPC's can be transversely polarized,[13–24] longitudinally polarized,[25] or without polarization but represented by time-dependent potentials.[26,27] In all these studies, the region acted upon by the time-dependent fields has dimensions shorter than the incoherent mean free path, so that electrons undergo predominately coherent inelastic scatterings within the region. Several interesting effects have been studied. First, the mechanism of time-modulated electron pumping has been proposed[13] in an unbiased asymmetric QPC, which is acted upon by a time-dependent transverse field. Second, the effects of photon-assisted processes on the quantum transport is studied.[14–20] The QPC considered is unbiased, has varying widths, and is acted upon by a time-dependent transverse field. More recently, QBS features are predicted to occur in a narrow constriction, which is acted upon by a time-dependent potential.[26,27] These QBS features are of similar physical origin as the impurity-induced QBS.[6–12]

Several methods have been developed to explore the time-modulated phenomena in QPC's. Earlier attempts expanded the scattering wave function in terms of the adiabatic wave functions of the QPC,[13,25] and converted the time-dependent Schrödinger equation into a set of coupled differential equations for the expansion coefficients. In striving for an analytic result, the authors had to ignore processes other than one- or two-photon processes. Later on, a hybrid recursive Green's-function method was proposed.[19,20] The formalism allows, in principle, multi-photon processes to be incorporated systematically and numerically up to many orders. However, their calculation has neglected the A^2 term in the Schrödinger equation, where **A** is the vector potential for the time-dependent electric field. Thus intrinsic two-photon processes have been neglected. Recently, a transfer-matrix method has been devised to study the effect of a longitudinally polarized time-dependent electric field on photon-assisted tunneling in double barrier structures.[28] The potential that represents the electric field was sliced into piecewise uniform potentials, and the method involved cascading the transfer matrices due to each of these piecewise uniform potentials. The focus of the work is on the scaling characteristics of the photon frequency in the photon-assisted tunneling. In this work, we focus on the QBS characteristics instead. By utilizing a vector potential to represent the electric field, we propose a matching scheme that avoids slicing the region

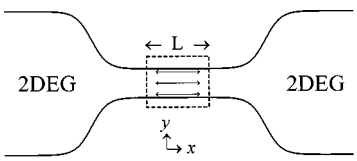

FIG. 1. Sketch of the gated QPC, which is connected at each end to a two-dimensional electron-gas electrode. The narrow constriction is acted upon by an external longitudinally polarized time-dependent electric field within millimeter wave range.

covered by the electric field. Thus our method is efficient and allows detail analysis of the QBS features.

We note here that the situations we considered are different from those in which the source and the drain electrodes are biased with an ac voltage.[29–31] In the latter situations, the time-dependent fields cover a region also including the reservoirs, which then is of a dimension longer than the incoherent mean free path. Whether the QBS features should remain robust in these latter situations is an interesting issue and is left to further study.

In this paper, we study the quantum transport in a narrow constriction, which is acted upon by an external time-dependent electric field. This electric field is chosen to be polarized longitudinally, with $\mathbf{E}(\mathbf{x},t)=\mathcal{E}_0\cos(\omega t)\Theta(L/2-|x|)\hat{x}$, where L denotes the range covered by the field and x represents the transmission direction. The finiteness in the range of the electric field breaks the translational invariance, and hence allows the coherent inelastic scatterings not to conserve the longitudinal momentum.[21,27] On the other hand, the uniformity of the electric field in the transverse direction allows only intrasubband transitions in the inelastic scattering processes and leaves the subband index n intact.

In the following we select the energy unit $E^*=\hbar^2k_F^2/(2m^*)$, the length unit $a^*=1/k_F$, the time unit $t^*=\hbar/E^*$, the frequency unit $\omega^*=1/t^*$, and the field amplitude $\mathcal{E}_0$ in units of $E^*/(ea^*)$. Here $-e$ denotes the charge of an electron, m^* represents the effective mass, and k_F is a typical Fermi wave vector of the reservoir. The time-dependent Hamiltonian is of the form $\mathcal{H}=\mathcal{H}_y+\mathcal{H}_x(t)$, where $\mathcal{H}_y=-\partial^2/\partial y^2+\omega_y^2y^2$ contains a quadratic confinement. The quantized transverse energy levels are $\varepsilon_n=(2n+1)\omega_y$, and the corresponding wave functions are denoted by $\phi_n(y)$.[32] The time-dependent part of the Hamiltonian $\mathcal{H}_x(t)$ is given by

$$\mathcal{H}_x(t)=-\left[\frac{\partial}{\partial x}-\frac{i\mathcal{E}_0}{\omega}\sin(\omega t)\Theta\left(\frac{L}{2}-|x|\right)\right]^2, \tag{1}$$

where the electric field is represented by a vector potential. For an nth subband electron incident upon the time-modulated region from the left reservoir with a total energy μ, the scattering wave functions are of the form $\Psi_n^+(\mathbf{x},t)=\psi(x,t,\mu_n)\phi_n(y)\exp(-i\mu_nt)$, where $\mu_n=\mu-\varepsilon_n$, and the subband index remains unchanged. The longitudinal part $\psi(x,t,\mu_n)$ of the scattering wave function can be casted into the form

$$\psi(x,t,\mu_n)=\exp\left[\frac{i\mathcal{E}_0^2}{4\omega^3}\sin(2\omega t)\right]\times\exp\left[\frac{-2\mathcal{E}_0}{\omega^2}\cos(\omega t)\frac{\partial}{\partial x}\right]\varphi(x,t,\mu_n), \tag{2}$$

which, when being substituted into Eq. (1) in the time-modulated region, would lead to an effective Schrödinger equation for $\varphi(x,t,\mu_n)$, given by

$$i\frac{\partial}{\partial t}\varphi(x,t,\mu_n)=\left[-\frac{\partial^2}{\partial x^2}+\frac{\mathcal{E}_0^2}{2\omega^2}\right]\varphi(x,t,\mu_n). \tag{3}$$

The effective Schrödinger equation (3) satisfied by $\varphi(x,t,\mu_n)$ has a constant potential term $\mathcal{E}_0^2/2\omega^2$, which is from the square of the vector potential. This suggests that the electric field causes an effective potential barrier in the time-modulated region, and this potential barrier depends on the amplitude and the frequency of the electric field. Making use of the complete set of the $\varphi(x,t,\mu_n)$ functions, we can write down the general form of the longitudinal wave function $\psi(x,t,\mu_n)$ in the time-modulated region. Along the entire x axis, the wave function $\psi(x,t,\mu_n)$ can be written in the following form:

$$\psi(x,t,\mu_n)=e^{-i\mu_nt}\left\{e^{ik(\mu_n)x}+\sum_m r_m(\mu_n)e^{-ik(\mu_n+m\omega)x}e^{-im\omega t}\right\}\quad \text{if } x<-\frac{L}{2}, \tag{4a}$$

$$\psi(x,t,\mu_n)=\int d\epsilon\left\{\tilde{A}(\epsilon)\exp\left[ik(\epsilon)\left(x-\frac{2\mathcal{E}_0}{\omega^2}\cos(\omega t)\right)\right]+\tilde{B}(\epsilon)\exp\left[-ik(\epsilon)\left(x-\frac{2\mathcal{E}_0}{\omega^2}\cos(\omega t)\right)\right]\right\}\times\exp\left[-i\left(\epsilon+\frac{\mathcal{E}_0^2}{2\omega^2}\right)t\right]\exp\left[\frac{i\mathcal{E}_0^2}{4\omega^3}\sin(2\omega t)\right]\quad \text{if } |x|<\frac{L}{2}, \tag{4b}$$

$$\psi(x,t,\mu_n)=\sum_m t_m(\mu_n)e^{ik(\mu_n+m\omega)x}e^{-i(\mu_n+m\omega)t}\quad \text{if } x>\frac{L}{2}. \tag{4c}$$

Here $k(\epsilon)=\sqrt{\epsilon}$ denotes the effective wave vector along $\hat{x}$ for an electron with energy ϵ. To facilitate the matching of the wave functions at all times, we write $\tilde{A}(\epsilon)$ and $\tilde{B}(\epsilon)$ in the form

$$\tilde{\mathcal{F}}(\epsilon)=\sum_m \mathcal{F}(m)\,\delta\left(\epsilon+\frac{\mathcal{E}_0^2}{2\omega^2}-\mu_n-m\omega\right), \tag{5}$$

where $\tilde{\mathcal{F}}(\epsilon)$ refers to either $\tilde{A}(\epsilon)$ or $\tilde{B}(\epsilon)$. Substituting Eq. (5) into Eq. (4c) and using the identities $\exp[-iz\sin(\omega t)]=\Sigma_mJ_m(z)\exp(-im\omega t)$, and $\exp[-iz\cos(\omega t)]=\Sigma_mJ_m(z)(-i)^m\exp(im\omega t)$, where $J_m(z)$ is a Bessel function, the boundary conditions for $\psi(x,t,\mu_n)$, which is continuous at $x=\pm L/2$, and for the derivative of $\psi(x,t,\mu_n)$ given by

$$-\left.\frac{\partial\psi}{\partial x}\right|_{x=\pm L/2+\delta}+\left.\frac{\partial\psi}{\partial x}\right|_{x=\pm L/2-\delta}\mp\frac{i\mathcal{E}_0}{\omega}\sin(\omega t)\psi\left(x=\pm\frac{L}{2},t,\mu_n\right)=0 \tag{6}$$

can be imposed. After some algebra, we obtain the equations relating $A(m)$, $B(m)$, and the transmission coefficients $t_m(\mu_n)$ given by

$$t_m(\mu_n)e^{ik(\mu_n+m\omega)L/2}=\sum_{m'} A(m')e^{i\beta(\mu_n+m'\omega)L/2}\sum_r J_r\left(\frac{\mathcal{E}_0^2}{4\omega^3}\right)J_{m'-m-2r}\left[\frac{2\mathcal{E}_0}{\omega^2}\beta(\mu_n+m'\omega)\right](-i)^{m'-m-2r}$$
$$+\sum_{m'} B(m')e^{-i\beta(\mu_n+m'\omega)L/2}\sum_r J_r\left(\frac{\mathcal{E}_0^2}{4\omega^3}\right)J_{m-m'+2r}\left[\frac{2\mathcal{E}_0}{\omega^2}\beta(\mu_n+m'\omega)\right](-i)^{m-m'+2r}, \tag{7}$$

$$k(\mu_n+m\omega)t_m(\mu_n)e^{ik(\mu_n+m\omega)L/2}=\sum_{m'} A(m')e^{i\beta(\mu_n+m'\omega)L/2}\sum_r J_r\left(\frac{\mathcal{E}_0^2}{4\omega^3}\right)\left\{\beta(\mu_n+m'\omega)J_{m'-m-2r}\left[\frac{2\mathcal{E}_0}{\omega^2}\beta(\mu_n+m'\omega)\right]\right.$$
$$\times(-i)^{m'-m-2r}+\frac{i\mathcal{E}_0}{2\omega}J_{m'-m-2r-1}\left[\frac{2\mathcal{E}_0}{\omega^2}\beta(\mu_n+m'\omega)\right]$$
$$\left.\times(-i)^{m'-m-2r-1}-\frac{i\mathcal{E}_0}{2\omega}J_{m'-m-2r+1}\left[\frac{2\mathcal{E}_0}{\omega^2}\beta(\mu_n+m'\omega)\right](-i)^{m'-m-2r+1}\right\}$$
$$-\sum_{m'} B(m')e^{-i\beta(\mu_n+m'\omega)L/2}\sum_r J_r\left(\frac{\mathcal{E}_0^2}{4\omega^3}\right)\left\{\beta(\mu_n+m'\omega)J_{m-m'+2r}\left[\frac{2\mathcal{E}_0}{\omega^2}\beta(\mu_n+m'\omega)\right]\right.$$
$$\times(i)^{m-m'+2r}-\frac{i\mathcal{E}_0}{2\omega}J_{m-m'+2r+1}\left[\frac{2\mathcal{E}_0}{\omega^2}\beta(\mu_n+m'\omega)\right](i)^{m-m'+2r+1}+\frac{i\mathcal{E}_0}{2\omega}J_{m-m'+2r-1}$$
$$\left.\times\left[\frac{2\mathcal{E}_0}{\omega^2}\beta(\mu_n+m'\omega)\right](i)^{m-m'+2r-1}\right\}, \tag{8}$$

and

$$2\delta_{m,0}k(\mu_n)e^{-ik(\mu_n)L/2}=\sum_{m'} A(m')e^{-i\beta(\mu_n+m'\omega)L/2}\sum_r J_r\left(\frac{\mathcal{E}_0^2}{4\omega^3}\right)\left\{\mathcal{K}_n^+(m,m')J_{m'-m-2r}\left[\frac{2\mathcal{E}_0}{\omega^2}\beta(\mu_n+m'\omega)\right]\right.$$
$$\times(-i)^{m'-m-2r}+\frac{i\mathcal{E}_0}{2\omega}J_{m'-m-2r-1}\left[\frac{2\mathcal{E}_0}{\omega^2}\beta(\mu_n+m'\omega)\right](-i)^{m'-m-2r-1}-\frac{i\mathcal{E}_0}{2\omega}J_{m'-m-2r+1}$$
$$\left.\times\left[\frac{2\mathcal{E}_0}{\omega^2}\beta(\mu_n+m'\omega)\right](-i)^{m'-m-2r+1}\right\}+\sum_{m'} B(m')e^{i\beta(\mu_n+m'\omega)L/2}\sum_r J_r\left(\frac{\mathcal{E}_0^2}{4\omega^3}\right)$$
$$\times\left\{\mathcal{K}_n^-(m,m')J_{m-m'+2r}\left[\frac{2\mathcal{E}_0}{\omega^2}\beta(\mu_n+m'\omega)\right](i)^{m-m'+2r}+\frac{i\mathcal{E}_0}{2\omega}J_{m-m'+2r+1}\left[\frac{2\mathcal{E}_0}{\omega^2}\beta(\mu_n+m'\omega)\right]\right.$$
$$\left.\times(i)^{m-m'+2r+1}-\frac{i\mathcal{E}_0}{2\omega}J_{m-m'+2r-1}\left[\frac{2\mathcal{E}_0}{\omega^2}\beta(\mu_n+m'\omega)\right](i)^{m-m'+2r-1}\right\}, \tag{9}$$

where $\beta(\epsilon)=k[\epsilon-\mathcal{E}_0^2/(2\omega^2)]$ and $\mathcal{K}_n^{\pm}(m,m')=k(\mu_n+m\omega)\pm\beta(\mu_n+m'\omega)$. Equations (7)–(9) show that the coefficients depend on the field amplitude $\mathcal{E}_0$, the photon frequency ω, the range L of the time-modulated region, and the transverse confinement parameter ω_y.

The zero-temperature conductance is given by

$$G=\frac{2e^2}{h}\sum_{n=0}^{N-1}{\sum_m}' T_n^m, \tag{10}$$

where N denotes the total number of propagating subbands, and the primed summation indicates that the summation over the sidebands includes only those sideband processes m of which $k(\mu_n+m\omega)$ is real. The transmission probability T_n^m for an electron that is incident in the subband n and emerges the sideband m from the time-modulated region is given by

$$T_n^m=\left[\frac{k(\mu_n+m\omega)}{k(\mu_n)}\right]|t_m(\mu_n)|^2. \tag{11}$$

Solving Eqs. (7)–(9) we obtain the coefficients $t_m(\mu_n)$, $A(m)$, and $B(m)$. The reflection coefficient $r_m(\mu_n)$ is also calculated, and the conservation of current is checked.

In our numerical examples, the physical parameters are chosen to be that in a high mobility GaAs-$Al_xGa_{1-x}As$ het-

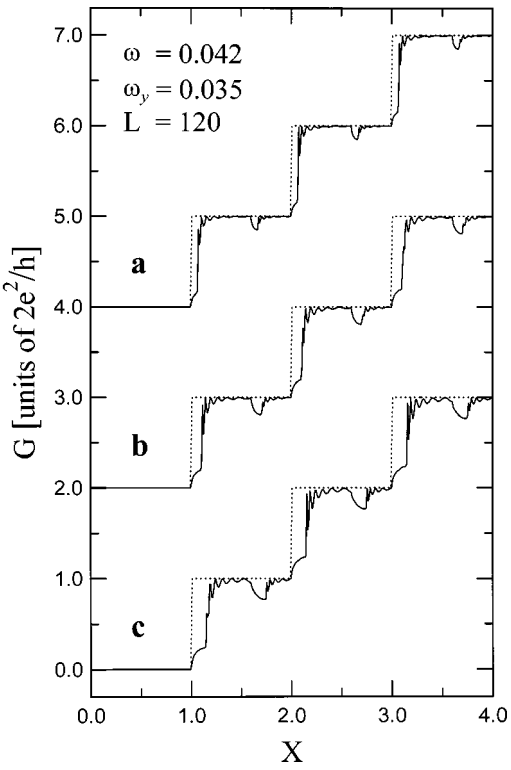

FIG. 2. Conductance G as a function of X for frequency $\omega = 0.042$ and $\omega_y = 0.035$ such that $\Delta X = 0.6$ when μ is changed by $\hbar\omega$. The length of the time-modulated region is chosen to be $L = 120$ ($\simeq 1$ μm). The amplitudes of the electric field are (a) $\mathcal{E}_0$, 0.004 ($\simeq$ 33.9 V/cm); (b) $\mathcal{E}_0 = 0.005$ ($\simeq$56.5 V/cm); and (c) $\mathcal{E}_0 = 0.006$ ($\simeq$67.8 V/cm). The curves are vertically offset for clarity.

erostructure, with a typical electron density $n \sim 2.5 \times 10^{11}$ cm^{-2} and $m^* = 0.067 m_e$. Correspondingly, we chose an energy unit $E^* = \hbar^2 k_F^2/(2m^*) = 9$ meV, a length unit $a^* = 1/k_F = 79.6$ Å, a frequency unit $\omega^* = E^*/\hbar = 13.6$ THz, and the field amplitude $\mathcal{E}_0$ in units of 11.3 kV/cm. In the following, the dependence of G on μ is more conveniently plotted as the dependence of G on X, where the integral value of

$$X = \frac{\mu}{\Delta\varepsilon} + \frac{1}{2} \tag{12}$$

gives the number of propagating channels. Here $\Delta\varepsilon = 2\omega_y$ is the subband energy-level spacing.

We present the G characteristics for three field amplitudes, with $\mathcal{E}_0 = 0.004$, 0.005, and 0.006 in Figs. 2(a)–2(c). Here we have chosen $\omega_y = 0.035$, such that the subband energy-level spacing $\Delta\varepsilon = 0.07$ and the effective narrow constriction width is of the order 10^3 Å. We also chose the field frequency $\omega = 0.042$ ($\nu = \omega/2\pi \cong 91$ GHz) and the length of the time-modulated region $L = 120$ ($\simeq 1$ μm). In the G versus X curves, $\Delta\mu = \hbar\omega$ corresponds to $\Delta X = \omega/\Delta\varepsilon = 0.6$. In addition, μ is at the Nth subband bottom when $X = N$.

From Fig. 2, G is found to exhibit two types of suppressed features—the valleylike structures in the plateau regions and the suppressed features near each integral value of X. The valleylike structures start with a cusp, at $X = 1.6$, 2.6, and 3.6, and end at an abrupt rise in G, at around $X + \Delta X_V$, where $\Delta X_V = 0.065$, 0.101, and 0.146, in Figs. 2(a)–2(c). On the other hand, the suppressed features near each integral value of X start at $X = N$, where G's suppression is large, with $|\Delta G| \lesssim 2e^2/h$, and end at around $N + \Delta X_V$, where G rises abruptly.

It is important to note that the widths ΔX_V of both types of the suppressed features are the same on the same curve when only μ, or X, is varying. Furthermore, these suppressed features are sensitive to the amplitude $\mathcal{E}_0$ and the frequency ω of the time-modulated field. In particular, we deduce, from our numerical results, an explicit field-dependent expression $\Delta X_V = \mathcal{E}_0^2/(2\omega^2\Delta\varepsilon)$ for the widths of these suppressed features. These findings about ΔX_V suggest that the widths for both types of the suppressed features must have been caused by the same physical factor.

To probe further into this physical factor, we would like to bring attention to two more facts. The first one is about the X locations of the cusps in the valleylike structures, which are at $N + \Delta X$. Recalling that ΔX corresponds to an energy of $\hbar\omega$, the incident electron in the Nth subband, and in this energy μ, can make an intrasubband transition to its unperturbed subband bottom by emitting one $\hbar\omega$. Such intrasubband transitions to a subband bottom have been shown to give rise to dip structures in G when a time-modulated potential acts upon a narrow channel.[27] These dip structures signify the trapping of the carriers by the QBS formed just beneath the subband bottom. Hence, the cusps in the valleylike structures must also be a manifestation of the QBS feature. However, the QBS feature found in this work is quite different from a dip structure. Instead of having G drops and rises within a very narrow energy width, G drops gradually over an energy interval ΔX_V before it rises again abruptly. Thus, even though both longitudinally polarized time-dependent fields and time-modulated potentials invoke only intrasubband transitions, they have different effects on the quantum transport.

The second fact we want to bring attention to is the oscillatory features in G. These oscillations are harmonics that arise from multiple scatterings between the two ends of the time-modulated region. The oscillation amplitudes increase with the field amplitude $\mathcal{E}_0$ while the oscillation pattern remains essentially the same. These harmonic oscillations appear and trail, on the higher-energy ends, every suppressed feature in G. In each of these oscillation patterns, the locations ΔX_n of the peaks, referenced to the higher-energy ends of the corresponding suppressed features, agree quite reasonably with that of the harmonic peaks, which ΔX_n are given by $(n\pi/L)^2/\Delta\varepsilon$ and are of values 0.01, 0.039, 0.088, 0.157, 0.245, and 0.353 in Fig. 2. The locations X_n of these harmonic peaks, whether they are at $X_n = (N + \Delta X_V) + \Delta X_n$ or at $X_n = (N + \Delta X_V) + \Delta X + \Delta X_n$, suggest the existence of an effective subband threshold at $N + \Delta X_V$. The latter harmonic peaks are from electrons that have emitted an energy ΔX. Hence for each subband there are two thresholds; the unperturbed threshold at $X = N$ and the effective threshold at $X = N + \Delta X_V$.

From the above results, we are led to the conclusion that a potential barrier of height ΔX_V, in units of $\Delta\varepsilon$, must be involved. Such a potential barrier is found to originate from the longitudinally polarized time-modulated electric field. In the region acted upon by the time-modulated electric field, the vector potential $\mathbf{A}$ contributes an A^2 term, given by

$[\mathcal{E}_0 \sin(\omega t)/\omega]^2$, in the Hamiltonian in Eq. (1). This term can be written in the form $(\mathcal{E}_0^2/2\omega^2)[1-\cos(2\omega t)]$, which consists of a term for the potential and a term that gives rise to 2ω processes. This is also the reason why such $\mathcal{E}_0^2/(2\omega^2)$ term appears in Eq. (3).

We have checked the above findings by solving the problem differently. Instead of describing the electric field by the vector potential **A**, we invoke a scalar potential of the form given by $-\mathcal{E}_0(x+L/2)\cos(\omega t)\Theta(L/2-|x|) - \mathcal{E}_0 L \cos(\omega t)\Theta(x-L/2)$. The method of solution is also different, which involves an extension of the scattering matrix approach to this time-dependent problem.[33] The results from both methods of solution are the same. Thus we have established all the features found in this work.

The existence of the static effective potential barrier $\mathcal{E}_0^2/(2\omega^2)$ due to the time-modulated electric field is not at all obvious if the electric field is represented by a scalar potential. It is natural, though, if the vector potential were invoked. Our previous studies show that a uniform oscillating potential alone does not produce an effective static potential barrier. The effective potential must then come from the longitudinal spatial variation in the oscillating scalar potential. On the other hand, we may ask whether similar features can be found when a uniform oscillating potential acts concurrently with a static potential barrier upon the constriction. We have calculated G for this case and find also in it both types of the suppressed features.[33] These understandings together provide us a coherent picture for the features found in this work.

The physical picture for the features in G is summarized in the following. As the longitudinally polarized time-modulated electric field acts upon the constriction, an effective potential ΔX_V is induced in the time-modulated region, thus setting up an effective potential barrier. The effective potential barrier causes a transmitting Nth subband electron, with incident energy $N \leqslant X < N+\Delta X_V$, to transmit via direct tunneling, or to transmit via assisted transmission by absorbing $m\Delta X$. The time-modulated region is very long so that transmission via direct tunneling is totally suppressed, leading to the large G suppression. For the assisted transmission, the electron has to tunnel into the time-modulated region first before it can absorb the needed energy. In Fig. 2, $\Delta X_V < \Delta X$, the minimum energy needed is ΔX. As X increases from N to $N+\Delta X_V$, the electron can tunnel deeper into the time-modulated region, so that the extent it obtains assistance is increased. Subsequently, G increases monotonically. The value of G saturates near $N+\Delta X_V$, showing that the saturated value of G, which increases with $\mathcal{E}_0$, is a measure of the effectiveness of the assisted process. In addition, the X region between N and $N+\Delta X_V$ is tunneling dominated, as shown by the absence of the harmonic structures.

When X increases beyond $N+\Delta X_V$, direct transmission process opens up, and G rises abruptly. Meanwhile, the electron with kinetic energy $X-(N+\Delta X_V)$ can perform multiple scattering between the two ends of the time-modulated region. This gives rise to the harmonic structures in G. When X is equal to $N+\Delta X$, a new process comes into play, and G exhibits a cusp structure. The electron can emit ΔX and reaches the QBS that is formed just beneath the subband bottom outside the time-modulated region. Again tunneling is involved, because the electron in the time-modulated region has to emit ΔX first, then tunnels out of the time-modulated region before it can reach the QBS. This process leads to a suppression in G, and it occurs more on the side of the time-modulated region where the electron is incident upon. This emit-then-tunnel process dominates the G characteristics in the region $N+\Delta X \leqslant X \leqslant N+\Delta X+\Delta X_V$. Within this X region, the tunneling range of the emit-then-tunnel process increases with X, so is the extent that the electron is involved in this process. Hence the suppression in G increases monotonically until its saturation near $N+\Delta X_V+\Delta X$. The maximum suppression in G is a measure of the effectiveness of the induced emission process. The abrupt rise in G at $N+\Delta X_V+\Delta X$ demonstrates that there is another QBS formed just beneath the effective subband threshold in the time-modulated region. The valleylike suppressed feature is resulted from the combined effects of the two QBS's. Finally, beyond $N+\Delta X_V+\Delta X$, the harmonic structure is dominated by the electrons that have emitted ΔX.

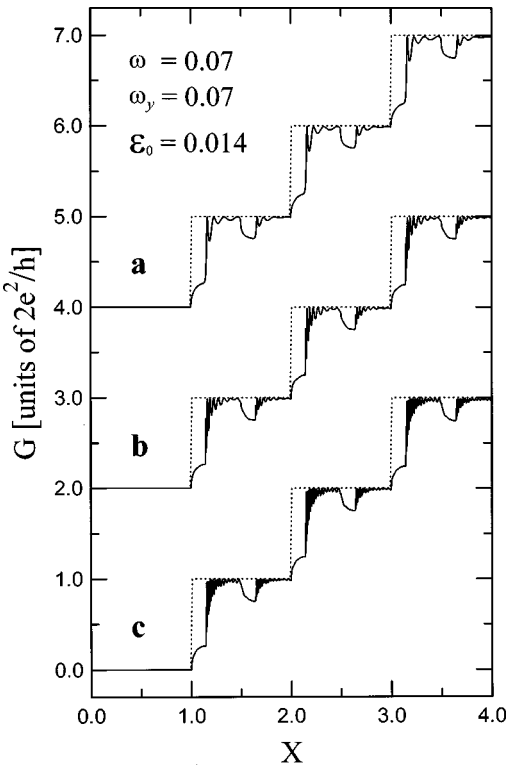

FIG. 3. Conductance G as a function of X for frequency $\omega = 0.07$ and $\omega_y = 0.07$ such that $\Delta X = 0.5$ when μ is changed by $\hbar\omega$. The field amplitude is chosen to be $\mathcal{E}_0 = 0.014$ ($\simeq 158.2$ V/cm). The lengths of the time-modulated regions are: (a) $L = 60$ ($\simeq 0.5$ μm); (b) $L = 120$ ($\simeq 1\mu$m); and (c) $L = 250$ ($\simeq 2$ μm). The curves are vertically offset for clarity.

In Fig. 3, we present the G characteristics for three lengths L of the time-modulated region with $L = 60$, 120, and 250 in Figs. 3(a)–3(c). Here we have chosen $\omega = \omega_y = 0.07$, such that $\Delta\varepsilon = 0.14$ and $\Delta X = 0.5$. The electric-field amplitude $\mathcal{E}_0 = 0.014$ such that $\Delta X_V = 0.143$. All the features discussed above can be found in these curves. In addition, except for the harmonic structures, the insensitivity of these features to L is clearly shown. The features will become sensitive to L only when it is short enough to allow appreciable direct tunneling.

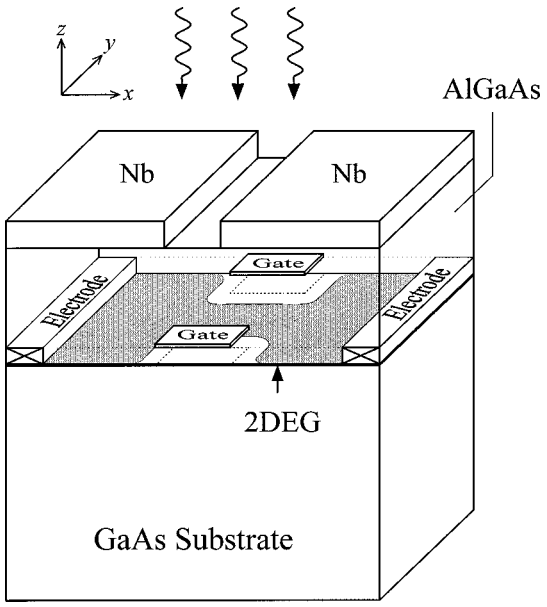

FIG. 4. Schematic illustration of our suggested experimental setup. Two Nb thin films separated between them by a submicron-sized gap are deposited on top of the split gate device. These films are at a submicron distance vertically above the split gates. The films and the split gates are separated by an insulating layer. In our numerical results, the incident electromagnetic waves are taken to be in the millimeter wave regime.

We note here that for the observation of the above predicted effects, the experimental setup needs to fulfill two requirements. First, the bolometric effect due to the absorption of photons in the QPC's end electrodes has to be suppressed or totally eliminated. Recent experiments show that the transport characteristics are masked by the bolometric effect when the entire QPC, including the end electrodes, is exposed to the incident electromagnetic field.[34] Second, in the above numerical examples, the length L of the region acted upon by the electromagnetic field is shorter than the wavelength of the incident field. The purpose is to increase the coupling between the electrons and the photons by breaking the longitudinal translational invariance. That the coupling between the photon field and the conduction electrons can be much enhanced, when either the electrons are confined or the electromagnetic field has a localized profile, has been pointed out recently by Yakubo *et al.*[35] Thus the QPC needs to be in the near-field regime of the electromagnetic field.

We suggest accordingly an experimental setup as shown schematically in Fig. 4. Two Nb thin films separated by a submicron gap are deposited on top of the split gate device. The films and the split gates are separated by an insulating layer of submicron thickness. The QPC, indicated by the shaded area, is then within the near-field regime when a millimeter electromagnetic wave is incident normally upon the device. For our purpose here, the incident field is longitudinally polarized, that is, the electric field is along the $\hat{x}$ direction. With this polarization, the two Nb films can function as an antenna. Since the QPC is in the near-field region of the antenna, the longitudinal field in the narrow constriction will have a profile localized in the longitudinal direction and is of submicron size.[36]

The Nb films have the added function of protecting the end electrodes from the incident millimeter electromagnetic wave. For the millimeter waves, the skin depth $\delta = 227$ nm at $T = 10$ K for a normal-state single-crystal Nb film.[37] This skin depth δ is expected to decrease with temperature, and to drop rapidly for $T < T_c$, when the film becomes superconducting.[38] The $T_c = 9.5$ K for bulk Nb, and $\hbar\omega/(2\Delta) \ll 1$ for millimeter waves.[37] Therefore, a Nb thin film of submicron thickness should be sufficient for keeping the electromagnetic wave from the end electrodes.

Given the availability of millimeter wave sources,[39] the suggested experimental setup would be manageable by the present nanotechnology. The features reported in this work, however, are not limited to millimeter waves.

In conclusion, we have found interesting field-sensitive suppressed features in G when a constriction is acted upon by a longitudinally polarized time-modulated field. The electric field is shown to induce a static potential barrier, which results in two QBS's for each subband. The interesting field-sensitive suppressed features occur whenever an electron can make intra-subband transition to the energies in between that of the two QBS's. In addition, we have demonstrated the nontrivial role that A^2 plays in affecting the quantum transport. We believe that the mechanisms studied in this work should find their way of manifestation in other time-modulated phenomena in mesoscopic structures, which system configurations are also within reach of the present nanotechnology.

The authors would like to thank Professor J. Y. Juang for useful discussions about our suggested experimental scheme. The authors also wish to acknowledge the National Science Council of the Republic of China for financially supporting this research under Contract No. NSC87-2112-M-009-007. Computational facilities supported by the National Center for High-Performance Computing are gratefully acknowledged.

[1] B.J. van Wees, H. van Houten, C.W.J. Beenakker, J.G. Williamson, L.P. Kouwenhoven, D. van der Marel, and C.T. Foxon, Phys. Rev. Lett. **60**, 848 (1988).

[2] D.A. Wharam, T.J. Thornton, R. Newbury, M. Pepper, H. Ahmed, J.E.F. Frost, D.G. Hasko, D.C. Peacock, D.A. Ritchie, and G.A.C. Jones, J. Phys. C **21**, L209 (1988).

[3] B.J. van Wees, L.P. Kouwenhoven, H. van Houten, C.W.J. Beenakker, J.E. Mooji, C.T. Foxon, and J.J. Harris, Phys. Rev. B **38**, 3625 (1988).

[4] L.I. Glazman, G.B. Lesovik, D.E. Khmelnitskii, and R.I. Shekhter, Pis'ma Zh. Éksp. Teor. Fiz. **48**, 329 (1988) [JETP Lett. **48**, 238 (1988)].

[5] L.I. Glazman and M. Jonson, Phys. Rev. B **41**, 10 686 (1990).

[6] C.S. Chu and R.S. Sorbello, Phys. Rev. B **40**, 5941 (1989).

[7] P.F. Bagwell, Phys. Rev. B **41**, 10 354 (1990).

[8] E. Tekman and S. Ciraci, Phys. Rev. B **43**, 7145 (1991).

[9] J.A. Nixon, J.H. Davies, and H.U. Baranger, Phys. Rev. B **43**, 12 638 (1991).

[10] Y.B. Levinson, M.I. Lubin, and E.V. Sukhorukov, Phys. Rev. B **45**, 11 936 (1992).
[11] Y. Takagaki and D.K. Ferry, Phys. Rev. B **46**, 15 218 (1992).
[12] Ch. Kunze and R. Lenk, Solid State Commun. **84**, 457 (1992).
[13] F. Hekking and Y.V. Nazarov, Phys. Rev. B **44**, 11 506 (1991).
[14] Q. Hu, Appl. Phys. Lett. **62**, 837 (1993).
[15] R.A. Wyss, C.C. Eugster, J.A. del Alamo, and Q. Hu, Appl. Phys. Lett. **63**, 1522 (1993).
[16] L. Fedichkin, V. Ryzhii, and V. V'yurkov, J. Phys.: Condens. Matter **5**, 6091 (1993).
[17] T.J.B.M. Janssen, J.C. Maan, J. Singleton, N.K. Patel, M. Pepper, J.E.F. Frost, D.A. Ritchie, and G.A.C. Jones, J. Phys.: Condens. Matter **6**, L163 (1994).
[18] L.Y. Gorelik, A. Grincwajg, V.Z. Kleiner, R.I. Shekhter, and M. Jonson, Phys. Rev. Lett. **73**, 2260 (1994).
[19] A. Grincwajg, L.Y. Gorelik, V.Z. Kleiner, and R.I. Shekhter, Phys. Rev. B **52**, 12 168 (1995).
[20] F.A. Maaø and L.Y. Gorelik, Phys. Rev. B **53**, 15 885 (1996).
[21] C.S. Chu and C.S. Tang, Solid State Commun. **97**, 119 (1996).
[22] Q. Hu, S. Verghese, R.A. Wyss, Th. Schäpers, J. del Alamo, S. Feng, K. Yakubo, M.J. Rooks, M.R. Melloch, and A. Förster, Semicond. Sci. Technol. **11**, 1888 (1996).
[23] Ola Tageman, L.Y. Gorelik, R.I. Shekter, and M. Jonson, J. Appl. Phys. **81**, 285 (1996).
[24] Ola Tageman and L.Y. Gorelik, J. Appl. Phys. **83**, 1513 (1997).
[25] S. Feng and Q. Hu, Phys. Rev. B **48**, 5354 (1993).
[26] P.F. Bagwell and R.K. Lake, Phys. Rev. B **46**, 15 329 (1992).
[27] C.S. Tang and C.S. Chu, Phys. Rev. B **53**, 4838 (1996).
[28] M. Wagner and W. Zwerger, Phys. Rev. B **55**, R10 217 (1997).
[29] M. Büttiker, J. Phys.: Condens. Matter **5**, 9361 (1993).
[30] T. Christen and M. Büttiker, Phys. Rev. Lett. **77**, 143 (1996).
[31] I.E. Aronov, G.P. Berman, D.K. Campbell, and S.V. Dudiy, J. Phys.: Condens. Matter **9**, 5089 (1997).
[32] M. Büttiker, Phys. Rev. B **41**, 7906 (1990).
[33] The method involves slicing the region acted upon by the electric field into piecewise uniform potentials, each covers the entire transverse dimension of the narrow constriction but has a narrow width along the longitudinal direction. The scattering matrix for each of these sliced scalar potentials can be obtained from our matching method. From cascading these scattering matrices, we can obtain the scattering matrix for the entire structure. The cascading scheme is very similar to that given by Ko and Inkson [Phys. Rev. B **38**, 9945 (1988)], except that we have to include, in addition, the sideband indices.
[34] J.A. del Alamo, C.C. Eugster, Q. Hu, M.R. Melloch, and M.J. Rooks, Superlattices Microstruct. **23**, 121 (1998).
[35] K. Yakubo, S. Feng, and Q. Hu, Phys. Rev. B **54**, 7987 (1996).
[36] When the wavelength λ of the millimeter wave is much larger than the submicron gap between the two Nb films, the transmitted electromagnetic wave is the same as the field generated by ac biasing the two films. It is clear then that the most significant field is within a submicron-sized region in the vicinity of the submicron gap.
[37] O. Klein, E.J. Nicol, K. Holczer, and G. Grüner, Phys. Rev. B **50**, 6307 (1994).
[38] This trend was demonstrated in NbN film by M. S. Pambianchi, S. M. Anlage, E. S. Hellman, E. H. Harford, M. Bruns, and S. Y. Lee, Appl. Phys. Lett. **64**, 244 (1994); B. Komiyama, Z. Wang, and M. Tonouchi, *ibid.* **68**, 562 (1996).
[39] See, for example, P. Bhartia and I.J. Bahl, *Millimeter Wave Engineering and Applications* (Wiley, New York, 1984), Chap. 3.